RSC Advances

ROYAL SOCIETY OF CHEMISTRY

www.rsc.org/advances

Manuscript ID: RA-ART-06-2014-005724

Title: "Synthesis of three-dimensional WO3 octahedra: Characterization, optical and efficient photocatalytic properties "

TOC

First time synthesized novel WO_3 octahedron microcrystals without using any surfactants/catalysts. The product exhibited photocatalytic performance of about 5.33 times greater than bulk which may be attributed to large surface area and highly reactive facet {120} of the exposed surface.

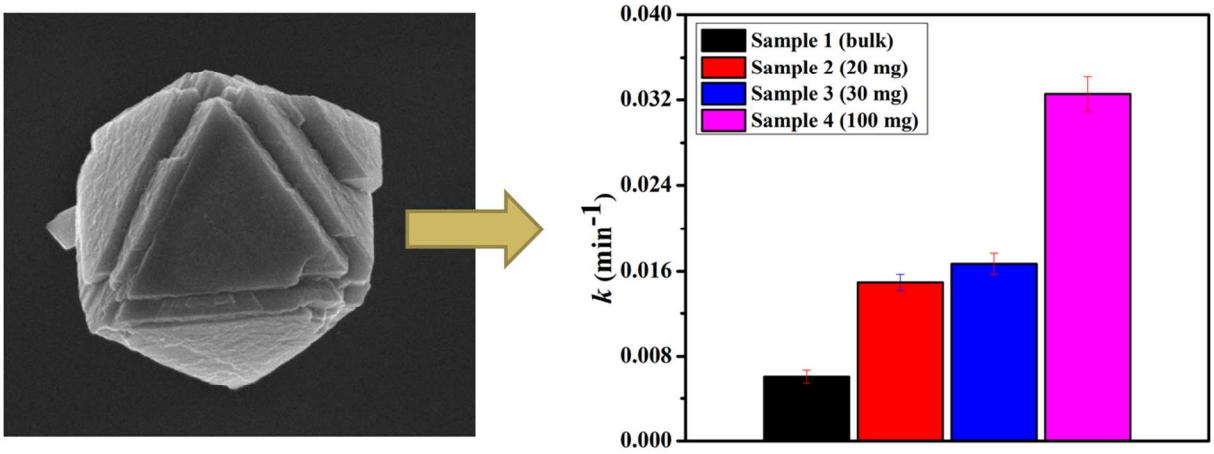

Cite this: DOI: 10.1039/c0xx00000x

www.rsc.org/xxxxxx

ARTICLE TYPE

Synthesis of three-dimensional WO_3 octahedra: Characterization, optical and efficient photocatalytic properties

Imran Aslam[a], Chuanbao Cao*[a], Waheed S. Khan[a], Muhammad Tanveer[a], M. Abid[b], Faryal Idrees[a], Rabia Riasat[c], Muhammad Tahir[a], Faheem K. Butt[a] and Zulfiqar Ali[a]

Received (in XXX, XXX) XthXXXXXXXXX 20XX, Accepted Xth XXXXXXXXX 20XX
DOI: 10.1039/b000000x

Three dimensional (3D) novel tungsten trioxide (WO_3) octahedra have been prepared by a simple surfactants/catalysts-free hydrothermal method. The phase and morphological structure of the as-synthesized material was analysed by X-ray diffraction (XRD), field emission scanning electron microscopy (FESEM), energy-dispersive X-ray (EDX) spectroscopy and X-ray photoelectron spectroscopy (XPS). FESEM results showed that the as-prepared WO_3 octahedron structure was in the range of 1-5 µm. Further, the optical properties like UV-VIS absorption spectrum, photoluminescence (PL) spectrum and Fourier transform infrared (FTIR) spectra of the product were also studied. The {120} side facet of the exposed surface of resulting product with large surface area (15.26 m^2/g), effective crystallinity and increased number of surface active sites exhibited excellent photocatalytic efficiency with higher rate constant (0.03254 min^{-1}) for the degradation of methylene blue (MB) under visible light irradiation. The photocatalytic performance of as-synthesized WO_3 octahedra was about 5.33 times greater than that of the bulk sample. The apparent excellent photocatalytic efficiency of the prepared sample can be attributed to large surface area and highly reactive {120} facet of exposed surface of WO_3 octahedra.

Introduction

In view of increasing demand for clean environment and cheap solar energy, semiconductor photocatalysts have received considerable interest over the last few decades. Among the various green chemical techniques, photocatalysis is one of the most promising techniques for the degradation of organic contaminants from wastewater and for renewable energy production as well [1-3]. Therefore, much attention has been paid on the semiconductor photocatalysis and significant efforts have been focussed to design new materials with band edge alignments suitable for photocatalytic reactions [4-9].

In the family of transitional metal oxides, tungsten trioxide (WO_3) with distinguished physical and chemical properties and broad applications, has received great attention because of its potential applications like visible-light-driven photocatalysts [10], water splitting [11], photochromic devices [12], and sensors [13]. As the physical and chemical properties of materials generally depend on the adopted synthesis route and their morphology, therefore it has been widely noticed that nano/micro morphology-based structured semiconductors, in comparison to bulk materials, exhibit more potential advantages in photocatalytic or photoelectrochemical cells applications because of their large surface area and size dependent properties including enhanced charge separation and migration, surface reactions and increased photon absorption [14, 15]. In past few decades, numerous kind morphologies of WO_3 including zero-dimensional (0D) WO_3 nanoparticles fabricated by condensation technique [16], one dimensional (1D) nano rods and nanowaires [17-19], two-dimensional (2D) nano films [20, 21], nano plates [22], nano flakes [23], nanotubes [24, 25], three dimensional hierarchical hollow shells [26] have been reported. Particularly, 2D and 3D nano/micro structures have received great interest in the field of material science due to their distinguished physicochemical properties. However, it is still a great challenge to synthesize and control 3D nanostructures of WO_3 as it requires a long reaction time and sometimes a complex procedure. Sonia *et al.* [27] synthesized twin octahedral structures of $WO_3.0.5H_2O$ by using sulfate salts based structure directing agents (SDAs) at a PH value of 5.25 and studied their Raman spectra. Zhao *et al*. [28] synthesized octahedral tungsten trioxide (with surface area 8.2 m^2/g) from commercially available WO_3 particles assisted by urea and found the photocatalytic activity 3.7 times than that of commercial WO_3. Very recently, the octahedral microcrystals of $WO_3.0.5H_2O$ have been reported and it was noted that the obtained microcrystals exhibited very good photocatalytic performance [29]. These days WO_3 has been paid much attention for its application as a photocatalyst because of relatively low band-gap energy (below 3.0 eV). Moreover, its strong absorption in the visible region at the wavelengths around 480 nm [30] makes it a good candidate for photocatalytic activities under solar light irradiation. This is the reason that WO_3 has been considered as a promising photocatalyst material which can be activated for the degradation of organic dyes or for hydrogen production under visible-light irradiation, like other alternative oxides such as $BiVO_4$ [31, 32], $CaIn_2O_4$ [33] and BiOBr [34] that exhibit better photocatalytic performance than that of traditional TiO_2. It has been observed that the photocatalytic reactivity of a semiconductor can be significantly affected by its electronic and surface atomic structures that are mainly dependent on the crystal

facet with different orientations [35]. Xie *et al*. [36] fabricated a quasi-cubic-like monoclinic WO_3 crystal with a nearly equal percentage of {002}, {200} and {020} facets and found the excellent O_2 evolution rate in the photocatalytic water oxidation. Moreover, they observed on the basis of surface energy {002} (1.56 J m^{-2}) > {020} (1.54 J m^{-2}) > {200} (1.43 J m^{-2}) that {200} is the most stable and {002} is the most unstable. However, the photocatalytic reaction mechanisms and the active sites at the catalyst surface of WO_3 are still not very clear and yet there is a challenge for researchers.

In the present work, we have successfully synthesized novel 3D pure WO_3 octahedra with large surface area for the first time via $Na_2WO_4.2H_2O$ and NaCl assisted by a very simple template-free hydrothermal method at a temperature of 180 ℃ without using any surfactants or catalysts. The as-sythesized WO_3 octahedra were utilized as photocatalyst for the degradation of organic dye methyl blue (MB) under visible light irradiation. The highly reactive {120} facet of the exposed surface of WO_3 octahedra presented the superior photocatalytic performance. Further, the obtained results were compared with bulk material and they showed distinguished photocatalytic performance and photo stability without any significant loss of efficiency upon recycling. In addition, we have also investigated the relationship between exposed surface of morphology and photoactivity properties.

Experimental Section

Fabrication of WO_3 octahedra

WO_3 octhedra were synthesized by hydrothermal growth method as follows:

Typically 1.0312 of $Na_2WO_4.2H_2O$ and 0.3712 g of NaCl were initially dissolved in 26 mL deionized water and magnetically stirred for 30 minutes, during the stirring add 4 mL of 2 M HCl dropwise, the greenish yellow colour solution was transferred into a 40 mL Teflon-lined stainless steel autoclave and kept it in the electric oven at 180 ˚C for 24 hours. As a result, a light gray colour powder was obtained which was then washed several times with distilled water and absolute ethanol respectively. The as-prepared material was dried at 80 ˚C for 18 hours and then calcined at 450 ˚C for 2 hours. The resulting product was saved for characterization and properties. In addition, the bulk material was also prepared for the comparison of results.

The as-synthesized WO_3 phase characterization was done by X-ray diffraction (XRD; Philips X'Pert Pro MPD), using a Cu Kα radiation source (λ = 0.15418 nm) with 2θ from 10˚ to 80˚. The morphology and composition of the as-prepared sample were analyzed by field emission scanning electron microscopy (FESEM), energy dispersive X-ray (EDX) analysis (Hitachi S-3500) and X-ray photoelectron spectroscopy (XPS). The Brunauer–Emmett–Teller (BET) specific surface area of the material was measured in a Micromeritics HYA2010-C2 (Beijing ZhongKe Hui Yu Technology Co., Ltd.) nitrogen adsorption instrument. The UV-VIS-NIR (Hitachi-4100) spectrophotometer was used to measure the optical absorption spectra and energy bandgap. PL spectrum was measured with a fluorescence spectrometer (Hitachi FL-4500) and Fourier transform infrared (FTIR) spectrum of sample was recorded using a Nicolet Avatar-370 spectrometer at room temperature.

Photocatalystic activity measurement

The photocatalytic test of the WO_3 octahedra sample was performed by degrading MB under visible light irradiation. For this purpose, an aqueous solution of MB (200 mL, 20 mg L^{-1}) was prepared and used different concentrations of the photocatalyst (20 mg, 30 mg and 100 mg) for the photodegradation of MB. The solution was placed in the dark at constant stirring for 30 min to attain the adsorption–desorption equilibrium between the photocatalysts and MB dye. It was then exposed to a 500 W tungsten halogen lamp (TrusTech, CHF-XM-500W) and at certain time intervals, 5 ml of the solution were taken and centrifuged before measuring the absorption. The UV–vis absorption spectra of the filtered solution were measured by using UV-VIS- NIR (Hitachi U-4100) spectrophotometer with initial wavelength at 603 nm.

Results and Discussion

Morphological characterization

The phase composition and crystal structure of the as-synthesized product were analyzed by powder X-ray diffraction. Fig. 1 (a) shows the XRD pattern of the WO_3 octahedron structure. All the diffraction peaks shown in Fig. 1 (a) were well matched with standard peaks of WO_3 (JCPDS Card No. 33-1387 with the lattice constants of a=b=7.298 Å, c=3.899 Å and α=β=90°, γ=120°) corresponding to (001), (200) and (201) planes *etc.,* diffraction at 2θ=22.798˚, 2θ=28.355˚ and 2θ=36.521˚ respectively. The lattice parameters of the as-synthesized structure were calculated by the equation $\frac{1}{d^2} = \frac{4}{3}[\frac{h^2+hk+k^2}{a^2}]+\frac{l^2}{c^2}$ using the crystal planes of (001) and (200), where d is interplanar spacing, *h, k, l* are Miller indices and *a, c* are the lattice constants respectively. The obtained calculated values a=b=7.3091 Å and c=3.911 Å were found to be in good agreement with the standard values. No others peaks of impurities or byproducts were observed, which indicates that the as-prepared sample is highly pure. The sharp, strong and narrow peaks show the good crystallinity of the sample. The strongest peak was observed at 2θ=28.355˚ corresponding to (200) planes. It can be seen from the XRD patterns that the crystallinity is much good and {200} is the dominant crystal facet, which shows that the crystals have been strongly grown along [200] direction and can be attributed to the intrinsic nature of a single crystalline WO_3 octahedra with dominant facet {200}. The chemical composition of the WO_3 octahedra was determined by employing EDX analysis. Fig. 1 (b) shows the EDX pattern of the fabricated sample which further confirms the composition of the elements existed in the sample. It can be seen clearly from Fig. 1 (b) that the as-prepared product contains only W and O elements, the Na peak in EDX may be due to the precursor (sodium tungstate) used in the synthesis process. The EDX analysis showed that that O and W exist in the product with a molar ratio of about 1:3 (W/O) which is cleared from Fig. 1 (b) and is in good agreement with XRD results.

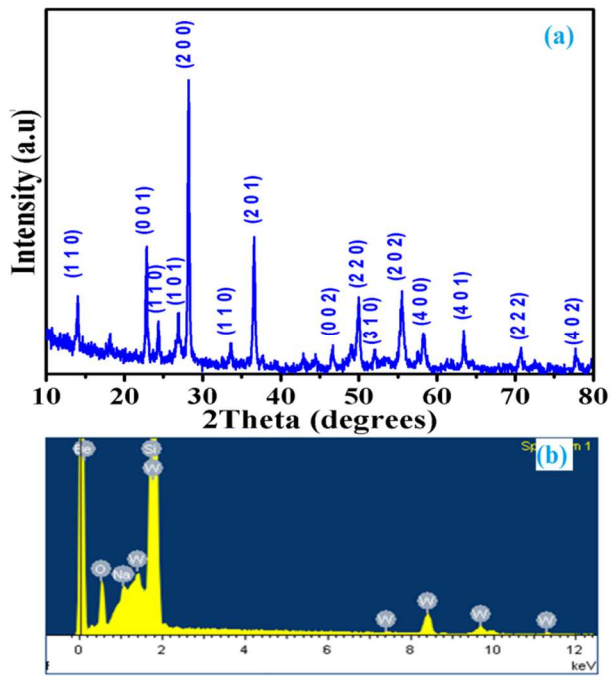

Figure 1 (a) X-ray diffraction pattern (XRD) of as-prepared WO_3 octahedra, and (b) EDX spectrum of the sample

The morphology, shape and size of the as-synthesized WO_3 sample were analyzed by using SEM as can be seen from Fig. 2. The Fig. 2 (a-d) shows the SEM images of WO_3 octahedra at different magnifications. The SEM images shown in Fig. 2 (a-d) depict that WO_3 microstructures are distributed at different orientations. It can be noticed that the as-prepared microstructures consist of eight faces like octahedron structure. Some of them are small and some are bigger in size, however, each crystal grain is a complete octahedron composed of eight equivalent triangular side facets as cleared from the high magnified FESEM image in Fig 3 b.

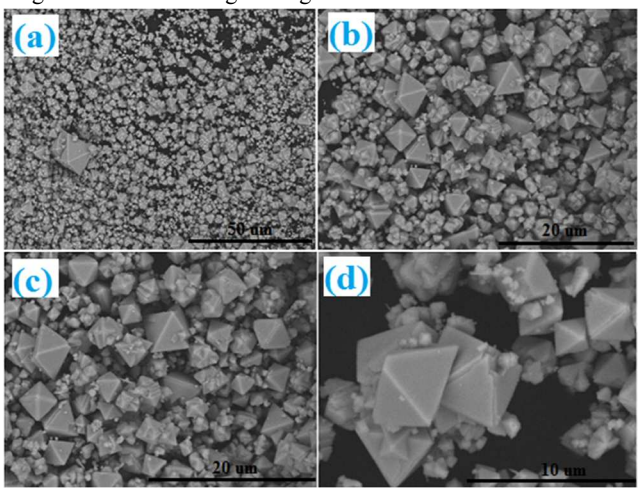

Figure 2 (a-d) SEM images of as-synthesized WO_3 octahedra at different magnifications

Fig. 3 (a, b) shows the FESEM images whereas Fig. (c, d) shows the TEM images of the of the product at different magnifications. Fig. 3 (a, b) shows a clear three dimensional (3D) view of the as-prepared samples. It can be noted that each octahedron type structure contains eight faces of which four are clear in Fig. 3 (b). In addition, it can also be noticed that the edge size of each octahedron microcrystal lies in the range of about 1 µm (Fig. 3 (b). The size and shape of the as-synthesized octahedra can be cleared further from the TEM images as shown in Fig. 3 (c and d).

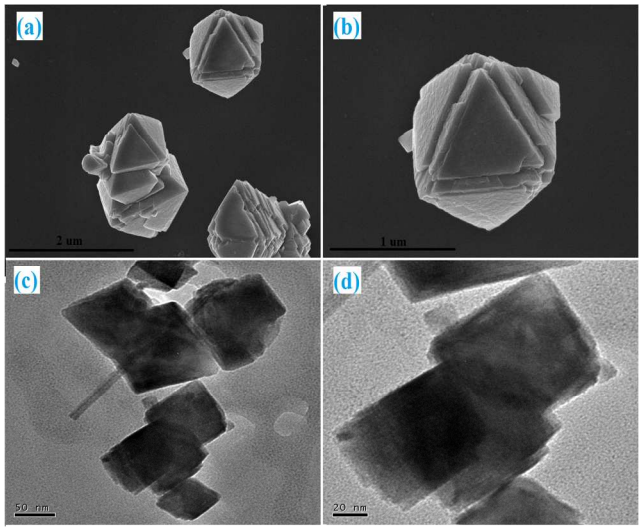

Figure 3 (a, b) FESEM images of WO_3 octahedra at different magnifications, and (c, d) TEM images of WO_3 octahedra at different magnifications

On the basis of SEM and TEM observations, it can be proposed that the surface of as prepared WO_3 octahedral crystal was composed of eight equal facets of which four {120}, {1-20}, {021}, and {02-1} facets are visible in diagram and the left four facets are respectively {-120}, {-1-20}, {0-21} and {0-2-1}. The {120} is the active exposed facet which mostly took part in the photocatalytic reaction. Moreover, it can be noted that from the centre of each octahedron, the six corners are situated along the [101], [-101], [10-1], [-10-1], [0-10], and [010] directions, respectively. A schematic explanation of the crystal orientation and facets of WO_3 octahedron is shown in Fig. 4.

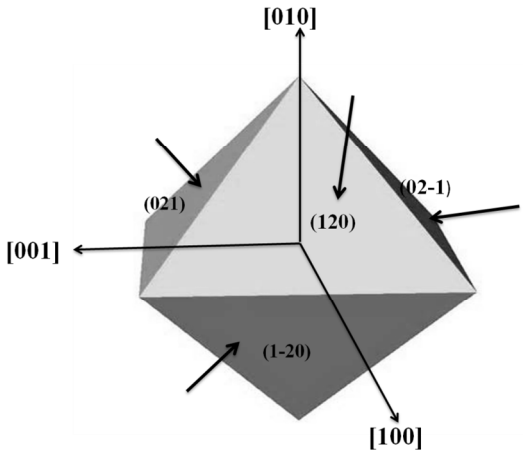

Figure 4 Schematic illustration of WO_3 octahedron with specific facets

XPS analysis

The elemental compositions and surface chemical states of the WO_3 octahedron microcrystals were examined by X-ray photoelectron spectroscopy (XPS). Fig. 5 presents the XPS spectra of the synthesized sample. A low-resolution full range XPS spectrum of the sample is shown in Fig. 5 (a). It provides the information about the chemical compositions and states of the synthesized WO_3 octahedra. The XPS analysis shows reveals that the prepared sample is composed of only tungsten and oxygen elements and no other impurity or byproduct was observed. The binding energy peaks corresponding to oxygen and tungsten can be clearly observed and there are no impurities other than carbon. The C1s peak appeared at 284 eV in the XPS results (Fig. 5 b) is due to the carbon paste which was used to stick the material on mount. The O1s peak (Fig. 5 c) positioned at 529.5 eV is associated with the oxide network with O^{-2} states in WO_3. Fig. 5 (d) reveals a complex energy distribution of W4f photoelectrons for tungsten. The W4f spectrum can be deconvoluted into a spin-orbit doublet corresponding to typical binding energies 34.7 eV and 36.8 eV resulted from the emission of $W4f_{7/2}$ and $W4f_{5/2}$ core-levels and may be attributed to tungsten atoms in W^{+5} oxidation state and are in good agreement with the reported results [37-39].

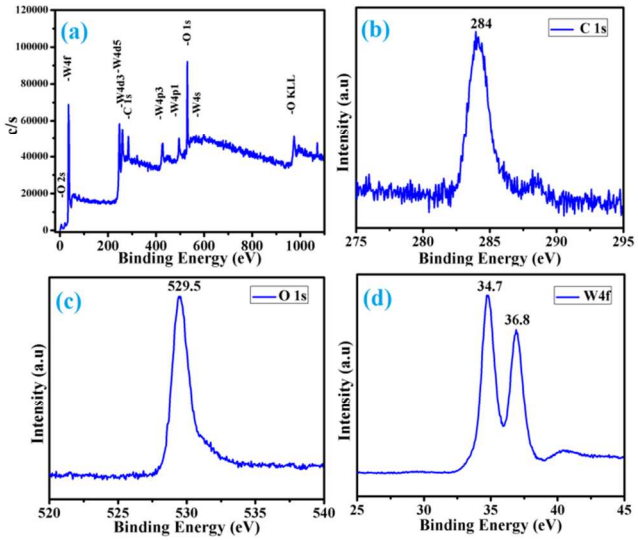

Figure 5 XPS surface spectra of as-synthesized product: (a) a full survey scan, (b) C 1s peak, (c) O 1s peak, and (d) W 4f peaks

FTIR and BET surface area

Further, the FTIR spectrum of product was examined in order to study the typical vibrations/modes of the synthesized product. Fig. 6 shows the FTIR spectrum of the WO_3 octahedra at room temperature. The absorption bands below 1000 cm^{-1} (like 749, 750, 813, 875 and 965 cm^{-1}) can be attributed to the different O–W–O stretching modes of pure WO_3 [40-44] and the peak at 1422 cm^{-1} is assumed as unusual value for OH stretching or OH bending modes, showing that OH groups have strong bonds either with water molecules or surface oxygen atoms [45]. The peaks at 1625 cm^{-1} [40, 46] and 1630 cm^{-1} [46, 47] are assigned to water bonded by oxygen atoms. Moreover, the peaks in the range 3200 3550 cm^{-1} can be ascribed to O–H stretching vibrations for WO_3 [40, 46].

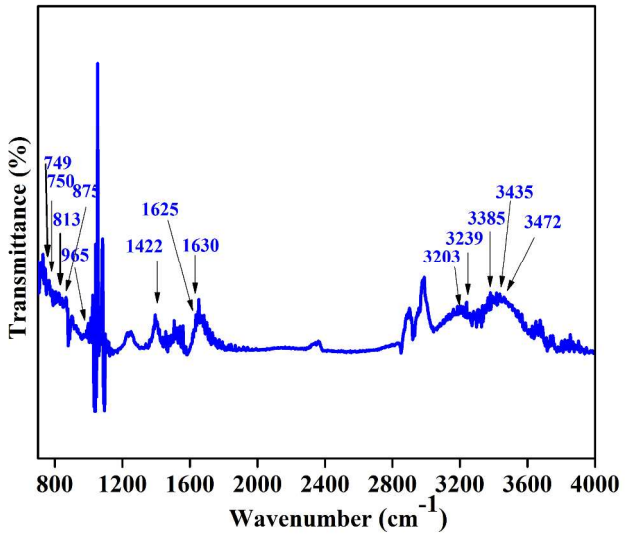

Figure 6 FTIR spectrum of the as-prepared WO_3 octahedra

For a good candidate of photocatalyst, the specific surface are of the material is an important aspect. It has been observed that surface area of the material plays an effective role in the photocatalytic process [48, 49] because the high surface area facilitates more active sites for photocatalytic reaction. The BET specific surface area of WO_3 octahedra was measured by nitrogen adsorption–desorption isotherm curves. Fig. 7 represents the nitrogen adsorption–desorption isotherms of the as-synthesized WO_3 octahedra and bulk. The BET specific surface areas for WO_3 octahedra and bulk were investigated as 15.26 m^2/g and 6.74 m^2/g, respectively. The large specific surface are of WO_3 octahedra thus resulted in superior photocatalytic activity and made it a promising catalyst for the decontamination of pollutants.

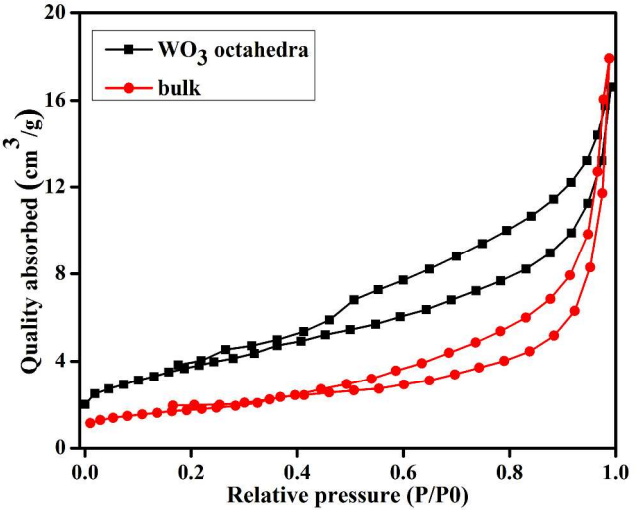

Figure 7 Nitrogen adsorption–desorption isotherms for WO_3 octahedra and bulk

Optical properties

The optical absorption of the final product was measured by UV–VIS–NIR spectrophotometer and by making the base-line with ethanol; the obtained data was plotted in the wavelength range 250-800 nm as shown in Fig. 8 (a). Using this absorption curve, the optical band gap of the octahedra was calculated as shown in the inset of Fig. 8 (*i.e.* Fig. 8 b). The optical absorption coefficient near the band edge obeys the following well known equation $(\alpha h\nu)^2=A(h\nu-Eg)$ for direct-bandgap, where α, h, ν, Eg, and A are the absorption coefficient, Planck's constant, frequency of light, band gap and a constant, respectively [50]. The bandgap was calculated as 2.84 eV (Fig. 8b) from the plot of $(\alpha h\nu)^2$ versus hν. The obtained band gap is thought much favorable for the photodegradation of organic pollutants under the visible light irradiation. Also the PL spectrum of the product was measured at an excitation wavelength of 280 nm as shown in Fig. 8 (c). It exhibits a strong violet emission peak centred at 437 nm (2.84 eV) corresponding to band-to-band transition by recombination of electrons from conduction band to the holes in valence band.

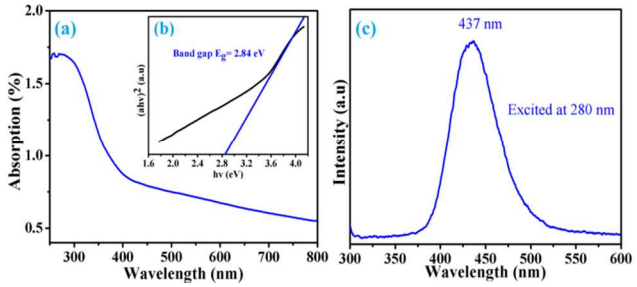

Figure 8 (a) The absorption curve of WO_3 octahedra, (b) The inset shows the optical bandgap graph of the as-synthesized octahedral, and (c) Room temperature PL spectrum of WO_3 octahedra

Photocatalytic property of WO_3 octahedra

It is well know that two steps are involved in the photodegradation of organic dyes, the adsorption of dye molecules, and secondly their degradation. The photocatalytic performance of the resulting product was tested by decomposing the MB dye under visible light source. The absorption spectra of the aqueous solution of MB in the presence of different concentrations (20 mg, 30 mg and 100 mg) of the as-synthesized WO_3 octahedra and percentage degradation along with corresponding rate constants under visible light irradiation at room temperature can be found in Fig. S1 (ESI†). The highest photocatalytic efficiency was achieved by sample 4 (*i.e.,* 100 mg) of WO_3 octahedra with a high rate constant 0.03254 min^{-1} and it degraded about 95 % of the dye in 60 minutes. Fig. 9 (a) shows the plot of ln (C_0/C) versus irradiation time, where C is the concentration of MB at any time *t* and C_0 is its initial concentration when adsorption-desorption equilibrium was attained while the Fig. 9 (b) shows pseudo-first order rate constants of all the samples respectively. The photodegradation of MB in the presence of sample material followed the pseudo-first order linear equation with reaction rate constant *k*. By the comparison of results from Fig. 9 (b), it could be found that the photocatalytic performance of the as-synthesized WO_3 octahedra (100 mg) was 5.33 times higher than that of the bulk which is the evidence of high photocatalytic efficiency of the product.

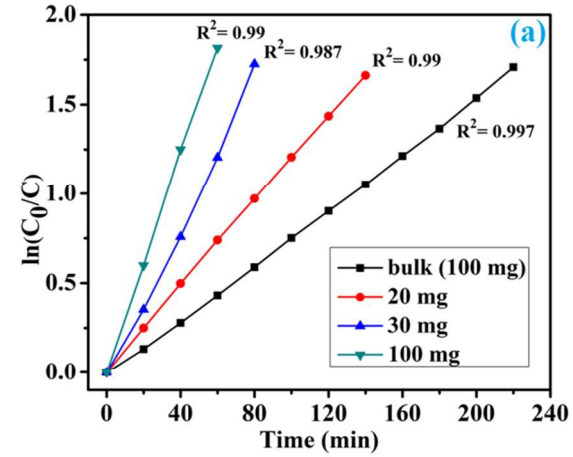

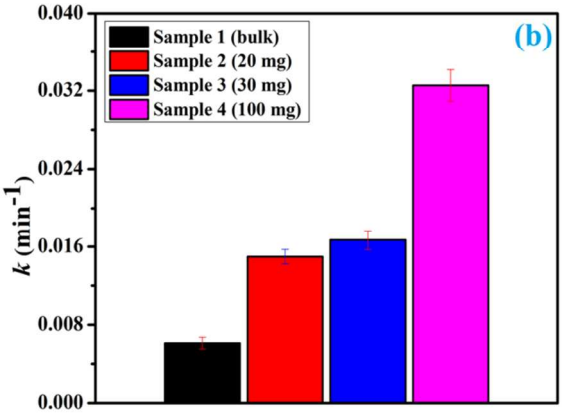

Figure 9 (a) The plot of ln (C_0/C) for all samples, and (b) The first-order rate constants for all samples

The determination coefficient (R^2) for all the samples of Fig. 9 (a), which explains the variability of response at a confidence level, was calculated according to the literature [51] and is given against each line. It was noted that the adjusted R^2 value was very close to 1, so the predicted values are in good agreement with the experimental data. The R^2 of the graph of ln (C_0/C) versus *t* for all samples were found to be greater than 0.95, therefore the experimental data fit the pseudo-first-order model in good manners. In Fig. 9 (b), the error bars are mentioned. The error bars indicates the standard deviations of triplicate experiments

It is well known fact that compared to bulk material, the specific morphology based materials show best properties. Moreover, the size and morphology of photocatalysts exert significant influences on their photocatalytic properties. Generally, for higher photocatalytic activity two things are more important; (i) high crystallinity (*i.e.,* less number of defects) which helps to reduce the photogenerated electron-hole pairs that take part in photocatalytic reaction, and (ii) large surface area that increases the number of active sites on the surface of photocatalyst [52,

53]. But, during the synthesis of metal oxides, it is often found difficult to satisfy these two requirements at the same time because to make a highly crystalline catalytic material high calcination temperatures are required which often reduce the specific surface area of the fabricated material. However, to attain these two conditions together is not impossible at all. Agarwala *et al*. [54, 55] group synthesized the mesoporous TiO_2 films and successfully obtained the highly crystallinity as well as the high surface area together in the presence of calcination temperatures. Therefore, to obtain an appropriate surface area and effective crstallinity, we have calcined the synthesized product at 450 ˚C for 2 hours. Thus, the fabricated octahedron structure of WO_3 maintained a large active surface area (15.26 m^2/g) which was favourable for photocatalytic degradation of MB, and provided more reaction sites and increased the efficiency of photogenerated charge carrier separation that resulted in the enhancement of charge-transfer rates in the photocatalyst. The photodegradation process of the semiconductors basically depends on the separation of photogenerated electron-hole pairs [31] and the transfer of separated electrons to the organic pollutant molecules. When a light of energy equal to or greater than the bandgap of WO_3 octahedra fell on their surface, the electron-hole pairs were generated, the electrons reacted with the neighboring O_2 to produce superoxide radicals ($\cdot O_2^-$) and at the same time holes reacted with water molecules on the photocatalyst surface to give rise highly reactive hydroxyl radicals (·OH). The formed $\cdot O_2^-$ and ·OH radicals finally degraded the organic dye. Herein, we have tried to study the influence of our WO_3 octahedra on the photocatalytic properties. For this purpose, we have degraded the methylene blue under the visible light irradiation. The absorption peak corresponding to MB was gradually decreased and almost disappeared after about 60 min, showing the excellent photocatalytic activity of exposed {120} reactive facet of the WO_3 octahedra as shown in Fig. S1 (d) (ESI†).. For comparison, the photodegradation of MB over bulk WO_3 sample was measured and also studied the effect of photolysis on MB decolorization under visible light at the same time. It was clearly observed that under the same experimental conditions, the exposed facet {120} octahedra of WO_3 exhibited the excellent photocatalytic properties as compared to bulk WO_3 sample that might be attributed to the high surface area, high crytallinity and as well as the increased number of surface active sites for octahedron microstructures. In addition, the exposed surface of the octahedron WO_3 microstructures might be more significant for their enhanced photocatalytic activities due to the increase in light transmission under visible light irradiation.

Conclusion

In summary, three dimensional tungsten trioxide (WO_3) novel octahedra were successfully synthesized by surfactants/catalysts-free hydrothermal method. FESEM results showed that the average size of octahedra was in the range of 1-5 µm. The optical bandgap with a value of 2.84 eV and room temperature PL spectrum were measured. The blue PL emission at 437 nm is attributed to band-to-band transition. The exposed facet {120} of WO_3 octahedra with large surface area (15.26 m^2/g), effective crystallinity and increased number of surface active sites exhibited superior photocatalytic performance for the degradation of MB under visible light irradiation. The photocatalytic activity of WO_3 octahedra was found 5.33 times greater in comparison to bulk material which can be ascribed to increased number of active sites due to high surface area.

ACKNOWLEDGMENT

This work was supported by National Natural Science Foundation of China (23171023，50972017) and the Research Fund for the Doctoral Program of Higher Education of China (20101101110026).

Notes and references

[a]Research Center of Materials Science, Beijing Institute of Technology, Beijing 100081, P. R. China.
Email: cbcao@bit.edu.cn;
[b]School of Physics, Beijing Institute of Technology, Beijing 100081, P. R. China.
[c]National Center for Nanoscience and Technology, Chinese Academy of Sciences, Beijing 100190, P. R. China.

Electronic Supplementary Information (ESI†) available: [Photodegradation curves of MB in the presence of WO_3 octahedra and bulk can be seen in Fig. S1].

[1] H. Tong, S. Ouyang, Y. Bi, N. Umezawa,M. Oshikiri,J. Ye, *Adv. Mater*., 2012, **24**, 229.
[2] R. Asahi, T. Morikawa, T. Ohwaki, K. Aoki, Y. Taga, *Science,* 2001, **293**, 269.
[3] R. Shi, J. Lin, Y. Wang, J. Xu and Y. Zhu, *J. Phys. Chem. C*, 2010, **114**, 6472.
[4] Y. H. Kim, H. Irie and K. Hashimoto, *Appl. Phys. Lett.*, 2008, **92**, 182107.
[5] M. G. Walter, E. L. Warren, J. R. McKone, S. W. Boettcher, Q. X. Mi, E. A. Santori and N. S. Lewis, *Chem. Rev.*, 2010, **110**, 6446.
[6] J. Z. Su, X. J. Feng, J. D. Sloppy, L. J. Guo and C. A. Grimes, *Nano Lett.*, 2011, **11**, 203.
[7] Muhammad Tahir, Chuanbao Cao, Faheem K. Butt, Sajid Butt, Faryal Idrees, Zulfiqar Ali, Imran Aslam, M. Tanveer, Asif Mahmood and Nasir Mahmood, *CrystEngComm*., 2014, **16**, 1825.
[8] Faryal Idrees, Chuanbao Cao, Faheem K. Butt, Muhammad Tahir, M. Tanveer, Imran Aslam, Zulfiqar Ali, Tariq Mahmood and Jianhua Hou, *CrystEngComm.*, 2013, **15**, 8146.
[9] M. Tanveer, Chuanbao Cao, Waheed S. Khan, Zulfiqar Ali, Imran Aslam, Faheem K. Butt, Faryal Idrees, Muhammad Tahir and Nasir Mahmood, *CrystEngComm.*, 2014, **16**, 5290.
[10] Z. G. Zhao and M. Miyauchi, *Angew. Chem. Int. Ed.*, 2008, **47**, 7051.
[11] R. Liu, Y. Yin, L. Y. Chou, S. W. Sheehan, W. He, F. Zhang, H. J. M. Hou and D. Wang, *Angew. Chem. Int. Ed.*, 2011, **50**, 499.
[12] S. Wang, X. Feng, J. Yao and L. Jiang, *Angew. Chem. Int. Ed.,* 2006, **45**, 1264.
[13] M. D'Arienzo, L. Armelao, C. M. Mari, S. Polizzi, R. Ruffo, R. Scotti and F. Morazzoni, *J. Am. Chem. Soc.,* 2011, **133**, 5296.

[14] R. Van De Krol, Y. Liang and J. Schoonman, *J. Mater. Chem*., 2008, **18**, 2311.
[15] A. I. Hochbaum and P. D. Yang, *Chem. Rev.*, 2010, **110**, 527.
[16] S. Li, I. N. Germanenko and M. S. El-Shall, *J. Phys. Chem. B*, 1998, **102**, 7319.
[17] S. L. Bai, K. W. Zhang, R. X. Luo, D. Q. Li, A. F. Chen and C. C. Liu, *J. Mater. Chem*., 2012, **22**, 12643.
[18] Bing Zhang, Chuanbao Cao, Hailin Qiu, Yajie Xu, Yingchun Wang and Hesun Zhu, *Chemistry Letters*, 2005, **34**, 154.
[19] S. Sun, Y. Zhao, Y. Xia, Z. Zou, G. Min, and Y. Zhu, *Nanotechnology,* 2008, **19**, 305709.
[20] C. Santato, M. Odziemkowski, M. Ulmann, J. Augustynski, *J. Am. Chem. Soc.,* 2001, **123**, 10639.
[21] S. H. Baeck, K. S. Choi, T. F. Jaramillo, G. D. Stucky, and E. W. McFarland, *Adv. Mater.,* 2003, **15**, 1269.
[22] D. Zhang, S. Wang, J. Zhu, H. Li and Y. Lu, *Appl. Catal. B,* 2012, **123**, 398.
[23] Y. He and Y. Zhao, *J. Phys. Chem. C,* 2008, **112**, 61.
[24] Z. Wang, S. Zhou and L. Wu, *Adv. Funct. Mater*., 2007, **17**, 1790.
[25] Kang Mingyang, Cao Chuanbao, Xu Xingyan and Lian Bo, *Chinese Res. Bull.*, 2008, **53**, 335.
[26] D. Chen and J. Ye, *Adv. Funct. Mater*., 2008, **18**, 1922.
[27] A. Sonia,Y. Djaoued, B. Subramanian, R. Jacques, M. Eric, B. Ralf and B. Achour, *Materials Chemistry and Physics*, 2012, **136**, 89.
[28] Z. G. Zhao, Z. F. Liu and M. Miyauchi, *Chem. Commun.,* 2010, **46**, 3323.
[29] J. Shi, G. Hu, R. Cong, H. Bu and N. Dai, *New J. Chem.,* 2013, **37**, 1544.
[30] K. Sayama, H. Hayashi, T. Arai, M. Yanagida, T. Gunji, and H. Sugihara, *Appl. Catal. B*, 2010, **94**, 150.
[31] A. Kudo, K. Omori, H. Kato, *J. Am. Chem. Soc.,* 1999, **121**, 11459.
[32] N. Castillo, L. Ding, A. Heel, T. Graule and C. Pulgarin, *Journal of Photochemistry and Photobiology A,* 2010, **216**, 221.
[33] J. Ding, S. Sun, J. Bao, Z. Luo and C. Gao, *Catal. Lett.,* 2009, 130, 147.
[34] Z. Jiang, F. Yang, G. Yang, L. Kong, M. Jones, T. Xiao and P. Edwards, *Journal of Photochemistry and Photobiology A*, 2010, **212**, 8.
[35] Jin You Zheng, Guang Song, Chang Woo Kim and Young Soo Kang, *Nanoscale*, 2013, **5**, 5279.
[36] Y. P. Xie, G. Liu, L. Yin and H. M. Chen, *J. Mater. Chem*., 2012, **22**, 6746.
[37] M. Sun, N. Xu, Y. W. Cao, J. N. Yao and E. G. Wang, *J. Mater. Res*., 2000, **15**, 927.
[38] B. A. Deangelis and M. Schiavello, *J. Solid State Chem.*, 1977, **21**, 67.
[39] A. P. Shpak, A. M. Korduban, M. M. Medvedskij and V. O. Kandyba, *J. Electron Spectrosc. Relat. Phenom.*, 2007, **156**, 172.
[40] H. I. S. Nogueira, A. M. V. Cavaleiro, J. Rocha, T. Trindade, and J. D. P. D. Jesus, *Mater. Res. Bull.*, 2004, **39**, 683.
[41] Guery, C. Choquet, F. Dujeancourt, J. M. Tarascon and J. C. Lassegues, *J. Solid State Electrochem.,* 1997, **1**, 199.
[42] C. Janáky, N. R. de Tacconi, W. Chanmanee and K. Rajeshwar, *J. Phys. Chem. C*, 2012, **116**, 19145.
[43] A. Baserga, V. Russo, F. Difonzo, A. Bailini, D. Cattaneo, C. Casari, A. Libassi and C. Bottani, *Thin Solid Films*, 2007, **515**, 6465.
[44] Z. J. Gu, T. Y. Zhai, B. F. Gao, X. H. Sheng, Y. B. Wang, H. B. Fu, Y. Ma and J. N. Yao, *J. Phys. Chem. B*, 2006, **110**, 23829.
[45] A. Phuruangrat, D. J. Ham, S. J. Hong, S. Thongtem and J. S. Lee, *J. Mater. Chem.*, 2010, **20**, 1683.
[46] W. Jiang, M. Pelaez, D. D. Dionysios, M. H. Entezari, D. Tsoutsou and K. O'Shea, *Chemical Engineering Journal,* 2013, **222**, 533.
[47] S. M. Kanan, Z. Lu, J. K. Cox, G. Bernhardt and C. P. Tripp, *Langmuir*, 2009, **18**, 1707.
[48] C. Ye, Y. Bando, G. Shen and D. Golberg, *J. Phys. Chem. B*, 2006, **110**, 15146.
[49] R. Narayanan and M. A. El-Sayed, *Nano Lett.* 2004, **4**, 1343.
[50] M. A. Butler, *J. Appl. Phys.,* 1977, **8**, 1914.
[51] Wenjun Jiang, Jeffrey A. Joens, Dionysios D. Dionysiou and Kevin E. O'Shea, *J. Photochem. Photobiol. A: Chem.,* 2013, **262**, 13.
[52] S. Ikeda, N. Sugiyama, S. Murakami, H. Kominami, Y. Kera, H. Noguchi, K. Uosaki, T. Torimoto and B. Ohtani, *Phys. Chem. Chem. Phys.*, 2003, **5**, 778.
[53] B. Ohtani and S. i. Nishimoto, *J. Phys. Chem.*, 1993, **97**, 920.
[54] S. Agarwala, M. Kevin, A. S. W. Wong, C. K. N. Peh, V. Thavasi, and G. W. Ho, *ACS Appl. Mater. Interfaces,* 2010, **2**, 1850.
[55] S. Agarwala, G. W. Ho, *Materials Letters*, 2009, **63**, 1627.